Experimental and CFD analysis of roll damping of a wind turbine installation vessel

Kjær, Rasmus Byrdal; Shao, Yanlin; Walther, Jens Honoré

Published in:
Applied Ocean Research

Link to article, DOI:
10.1016/j.apor.2023.103857

Publication date:
2024

Document Version
Publisher's PDF, also known as Version of record

Applied Ocean Research 143 (2024) 103857

Contents lists available at ScienceDirect

Applied Ocean Research

journal homepage: www.elsevier.com/locate/apor

Research paper

Experimental and CFD analysis of roll damping of a wind turbine installation vessel

Rasmus Byrdal Kjær [a,b], Yanlin Shao [b], Jens Honoré Walther [b,*]

[a] OSK Design, Bryggervangen 55, 1. th, Copenhagen OE, DK-2100, Denmark
[b] Department of Civil and Mechanical Engineering, Technical University of Denmark, Nils Koppels Allé, Kgs. Lyngby, DK-2800, Denmark

ARTICLE INFO

Keywords:
Computational fluid dynamics
Hydrodynamics
Roll motion
Roll damping
Wind turbine installation vessels
Seakeeping
Digital twin
Free roll decay
Model tests

ABSTRACT

The global transition to renewable energy has put pressure on wind turbine installation vessels (WTIV), thus creating an urgent demand for optimizing their operation. This includes more accurate predictions of the ship motions at sea, at which roll motion is of particular interest. For accurate prediction of the roll motion, roll damping is important to consider and is commonly found from empirical methods if experimental data are not available. Since the hull geometry and loading conditions of WTIVs are significantly different from conventional ships the validity of existing empirical methods has not been justified. This paper studies an alternative approach of determining the roll damping, by utilizing CFD to simulate free roll decay of a WTIV, from which the roll damping can be extracted. A WTIV is simulated under different loading conditions, varying the vertical center of gravity and adding a bilge keel to study the influence on the roll damping. Model tests are carried out to validate the CFD simulations. CFD simulations are performed in both model scale and full scale. The implied extreme roll motions in irregular waves are compared with empirical methods. It is found that CFD can predict roll damping accurately and that roll damping decreases for high centers of gravity. The viscous scaling effects for a 2 m long model is significant, causing too large damping in model scale. The investigated bilge keel reduced roll motions significantly. The empirical methods consistently overestimated the roll damping, especially near the resonant frequency.

1. Introduction

Wind turbine installation vessels (WTIVs) are vessels that are used for installing offshore wind turbines and is a key player in the establishment of offshore wind energy. Hence there is a need to optimize their operation in order to meet the demands in the global transition to renewable energy. WTIVs are characterized by having 4–6 legs which can be lowered down to the sea floor and jack-up the vessel to provide a fixed platform to install from. They typically have a wide breadth, which ensures large restoring moments, hence high stability that allows for a high vertical center of gravity, but also results in a shallow draught. A wide breadth and shallow draught are characteristics that are shared by barges. Contrary to most barges, WTIVs often have a high vertical center of gravity because of their tall jack-up legs, installation crane and the freight consisting of wind turbine towers, and stacked wind turbine wings. These characteristics not only affect the dynamic behaviour of the ship but also represent challenges in the prediction of the ship motions, in particular the roll motion. Roll motion is essential to predict because it represents the degree of freedom with the, by far, smallest moment of inertia, hence the most exposed degree of freedom to large motions. Throughout history severe roll motions of ships have led to countless accidents, whereas loss or damage of cargo is still a frequently occurring event. Thus to avoid such incidents in the offshore industry and to maximize their operation it is important to have accurate predictions of the roll motions of WTIVs.

Motion analyses of vessels, i.e., seakeeping problems, are essentially dealt with by solving the equations of motion for all six degrees of freedom in either the frequency or the time domain. When solving the equations of motion, the added mass and damping coefficients are usually calculated from potential flow theory, using strip theory or three-dimensional panel methods. These can predict the ship motions in waves to a fairly good accuracy for the motions in pitch and heave, which together with roll often represent the largest motions. Solving for roll motions using potential flow alone can be inaccurate due to significant viscous loads, with eddy making being the dominant factor. The eddies are formed at the turns of the bilge and appendages on the hull, as illustrated in Fig. 1. Therefore, empirical viscous roll damping, estimated by for instance the Ikeda's method (Himeno, 1981), is added into the roll motion equations to avoid nonphysical results

* Corresponding author.
E-mail addresses: rbk@oskdesign.com (R.B. Kjær), yshao@dtu.dk (Y. Shao), jhwa@dtu.dk (J.H. Walther).

https://doi.org/10.1016/j.apor.2023.103857
Received 3 July 2023; Received in revised form 29 October 2023; Accepted 20 December 2023

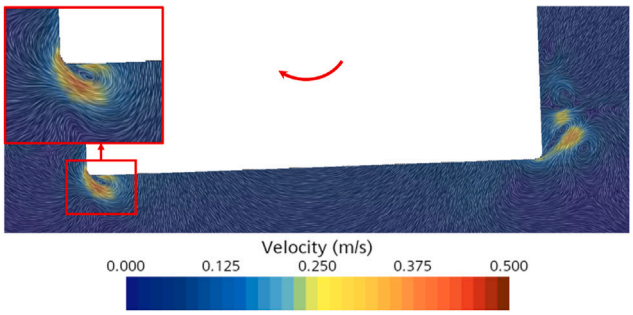

Fig. 1. Velocity field generated from a model scale CFD simulation, illustrating how eddies are formed at the downstream side of the turns of the bilge.

in the numerical prediction. Ikeda's method was developed in the late 1970s from an extensive experimental study conducted on models of conventional cargo ships. The roll damping is divided into components representing the different physical phenomena causing the damping. The method is one of the most widely used models for predicting roll damping and is implemented in many commercial software.

While Ikeda's method is fairly reliable for conventional ships, its validity is unclear for box-shaped vessels like barges and WTIVs. It was shown by Standing (1991) that Ikeda's original method underestimates the eddy roll damping for barges, and an adapted method was later developed specifically for barges and flat-bottomed shallow-draught vessels, which introduces more eddy roll damping. This adapted method is described in the ITTC 2011 procedure on prediction of roll damping (ITTC Specialist Committee et al., 2011), and will hereafter be referred to as the ITTC 2011 barge model. The ITTC 2011 also provides procedures for conventional ships based on Ikeda's method. Kawahara et al. (2011) found that Ikeda's method overestimates the roll damping for Wide breadth Shallow draught Pure Car Carriers (WSPCC). The WSPCC ship type is characterized by a high center of gravity relative to the draught, similar to WTIVs. Due to the shared characteristics of WTIVs and barges (wide breadth and shallow draught), the ITTC 2011 barge model seems like an obvious candidate when choosing a viscous roll damping model, if not for the high center of gravity of WTIVs, which may make the validity of the barge model questionable. Further, the findings of Kawahara et al. (2011) could indicate that the conventional Ikeda's method would overestimate the roll damping, making the barge model even less appropriate as it introduces more roll damping than the conventional Ikeda's method.

Over the years, the use Computational Fluid Dynamics (CFD) has been shown applicable as a method to study the roll damping of ships through numerous papers. The majority of the studies are carried out on two-dimensional hull sections, but in recent years a number of papers have studied roll damping on three-dimensional hulls as well. The most relevant papers are covered briefly here. Irkal et al. (2016) studied roll damping of a two-dimensional ship cross section with various bilge keels using CFD and with experimental validation. The study was carried out in model scale and the roll damping was estimated from free-decay simulations. CFD results replicated experimental results to a high accuracy. Further, it was found that the roll damping with bilge keels is non-linear and that the non-linearity increases with the size of the bilge keel. Devolder et al. (2020) investigated roll damping on an offshore heavy lift installation vessel in CFD using OpenFOAM by simulating forced roll tests for a number of different amplitudes, roll periods and forward speeds. All simulations were carried out with the same loading condition and in full scale. No validation against full scale measurements or experimental tests was provided. Ghamari et al. (2022) studied the use of CFD as a method to extract roll damping of a fishing vessel by simulating free roll decay tests (three-dimensional hull) in model scale. CFD results were validated against experimental tests, which showed a high level of accuracy. Quadratic damping coefficients were extracted and applied in a potential flow based seakeeping model to investigate parametric roll of the ship. Compared with experimental results the obtained results showed a satisfactorily agreement. Kianejad et al. (2018) simulated forced roll tests (harmonic excited roll motion) on a post-Panamax container ship in CFD using the commercial software *STAR CCM+*. The ship was excited with moments corresponding to beam and oblique sea under different frequencies, degrees of freedom and forward speeds. Roll damping coefficients were to some extend compared to experimental results, which showed good agreement for frequencies smaller than or close the roll resonance frequency.

Recent publications on CFD-derived roll damping, including the above described, have proven the general applicability of the concept. The research on CFD-derived roll damping of WTIVs is however very limited and none of the found studies included experimental validation. Furthermore, studies on the validation of the widely used empirical methods are lacking for WTIVs. In general, there is a gap in validating widely-used empirical methods when applied to WTIVs. The industry faces the challenge of accurately estimating roll damping and predicting roll motions for WTIVs in waves. This knowledge gap raises questions about the effectiveness of existing empirical roll damping models. An inadequate model can lead to safety concerns or overly conservative operational limitations. Another concern is the scale effect when extrapolating model-test results to full scale applications, as the Reynolds numbers and thus the flow physics are significantly different in model and full scale. Further research in this area is crucial to address these uncertainties and improve the operational safety and efficiency of WTIVs.

For other ship types and ship-shaped FPSO (Floating Production Storage and Offloading), bilge keels are often used to increase the roll damping and thus significantly reduce the roll motions in waves. Currently, they are generally not used on existing WTIVs. However, adding bilge keels could potentially extend the operational weather window for the vessels as well as reduce grillage costs. It has not been attempted in the literature to quantify the effects in reducing roll motions of WTIVs by adding bilge keels to bare hull.

In this study, we present an extensive and thorough study of the roll damping and the influence of the vertical center of gravity (COG), in both model and full scale, and using both numerical and experimental approaches. Specifically, a three-dimensional CFD model for the considered WTIV is developed in *STAR CCM+*, from which the roll damping is calculated by simulating roll decay tests in the time domain, initially in model scale to validate against model tests and later in full scale. Model tests are conducted under different loading conditions to verify the reliability and accuracy of the CFD model, as well as to study the influence of the COG on the roll damping. Extracted roll damping coefficients are applied in a potential flow based seakeeping analysis and are compared to the Ikeda-based roll damping models, recommended by the ITTC 2011 procedures (ITTC Specialist Committee et al., 2011). To enlighten the discussion on the use of bilge keels on WTIVs, this is studied from a conceptual point of view.

2. Experimental and CFD modelling

2.1. Methodology

If a single-degree-of-freedom roll motion is considered, the equation of motion may be represented as:

$$(M_{44} + A_{44})\ddot{\phi} + B_{44}\dot{\phi} + C_{44}\phi = F_4(\omega t). \quad (1)$$

Here, M_{44} is the moment of inertia, A_{44} is the added mass (from the water), B_{44} is the linearized roll damping coefficient, C_{44} is the restoring force coefficient, and $\ddot{\phi}$, $\dot{\phi}$, and ϕ are respectively the angular acceleration, velocity and position of the vessel. This paper is concerning the determination of B_{44} which in its nature is non-linear and dependent on both amplitude and frequency of the roll motion (Himeno, 1981).

The roll damping may be determined from Ikeda's method (Himeno, 1981) as a summation of damping components:

$$B_e = B_F + B_E + B_W + B_L + B_{BK}, \tag{2}$$

where B_F is skin-friction, B_E is eddy-making, B_W is wave-making, B_L is a contribution from lift force (only present at forwards speed), and B_{BK} is the additional damping from the bilge keel, if one is present. The friction and eddy components, B_F and B_E, represent the viscous parts, while the wave and lift components, B_W and B_L, represent the non-viscous parts of the damping. The bilge keel component contains both viscous and non-viscous parts. The distribution of the damping between the components is difficult to quantify, generally because it varies significantly with the hull shape. Since the roll damping is non-linear and dependent on both roll amplitude and frequency, the second term in Eq. (1) is insufficient and a better representation of the second term would be to express the damping moment as a function of the roll velocity $B_\phi(\dot{\phi})$ (Himeno, 1981), thus the damping can be expressed in a non-linear form as a series expansion of the roll velocity as

$$B_\phi = B_1\dot{\phi} + B_2\dot{\phi}|\dot{\phi}| + B_3\dot{\phi}^3 + \cdots \tag{3}$$

where the coefficients B_1, B_2 etc. are considered constant during the motion. Often only B_1 and B_2, or the quadratic damping B_2 alone, are considered. These coefficients can be obtained from experimental results or CFD simulations of free decay tests. The general form of expressing the non-dimensional damping coefficients from a free decay is given in Eq. (4), where the relationship with the dimensional equivalent linear damping is also given. Note that this is true for $\zeta \ll 1$.

$$\zeta = \frac{1}{2\pi N}\log\left(\frac{\phi_i}{\phi_{i+N}}\right) = \frac{B_{44}}{2(M_{44}+A_{44})\omega_n}, \tag{4}$$

where ϕ_i is the amplitude of the i-th peak, N is the number of oscillations for which the damping is linearized over and ω_n is the natural frequency. Non-linear damping coefficients can be extracted in more than one way. This paper shall follow the procedure outlined by Faltinsen (1993). In this procedure, it is assumed that the roll can be described as a 1-DOF motion and that the damping is defined by the logarithmic approach from Eq. (4). Assuming a constant relationship between the damping and the amplitude of the oscillation, the non-dimensional linear and quadratic damping coefficients b_1 and b_2 can be determined from:

$$\frac{2}{T_{n4}}\log\left(\frac{\phi_{i-1}}{\phi_{i+1}}\right) = b_1 + \frac{16}{3}\frac{\phi_i}{T_{n4}}b_2. \tag{5}$$

Note that there is one half period between ϕ_i and ϕ_{i+1} for any i. The extracted damping coefficients might not be accurate in the entire decay process, because it is difficult and sometimes impossible to fit a straight line that will be valid for the total decay time. This is especially the case if the drag coefficient (hence the damping force) is strongly dependent on the Keulegan–Carpenter (KC) number or the Reynolds number (Faltinsen, 1993).

2.2. Model tests

Roll damping can be obtained experimentally either by forced roll or by free roll decay. Forced roll tests enable measurement of the roll damping at any combination of frequency and amplitude, but require a substantially more extensive test setup. Free roll decay is a simpler setup, where the ship is inclined to an initial heel angle and then released to roll freely. The main drawback of this setup is that the model will always roll at the natural frequency, thus the damping cannot be examined at other frequencies. In free decay tests the ship is often restrained from sway and yaw motions to avoid the effects of horizontal motions. In such case the roll axis is assumed coincident with the center of gravity. In this study the experiments were conducted as free roll decay test but not restrained from swaying, as this will also be the case in reality. The study was conducted on a scaled model of the vessel *Wind Orca*, owned and operated by *Cadeler A/S* and among the largest WTIVs in the world. The principal dimensions of the vessel are listed in Table 1. Note that full scale mass properties are non-dimensionalized throughout this paper, according to definitions in Supplementary 3, to protect *Cadeler* from misinterpretation of sensitive data.

Table 1
Principal dimensions and mass properties of the *Wind Orca*. COG is given in a global coordinate system (GCS).[1] Abbreviations: LWL (length of water line), Lpp (length between perpendiculars).

Model scale	1:80	
Parameter	Full scale	Model scale
LWL	160 m	2 m
Lpp	155.6 m	1.945 m
Breadth (moulded)	49 m	0.6125 m
Design draught	5.5 m	0.06875 m
Max draught	6 m	0.075 m
Block coefficient C_b	0.831	0.831
Metacentric height $\overline{GM}_T$[a]	0.408	0.250 m

[a] At base loading condition, draught 5.5 m (see Table 2). Non-dimensionalized in full scale, according to Supplementary 3.

Fig. 2. Ship model of *Wind Orca*, launched into the basin, loaded to max draught.

Tests were conducted at the testing facility at the *Technical University of Denmark* (DTU) in a water basin of dimensions (3 m × 35 m). A scaled model of the ship was built from scratch and its dimensions were defined to fit the pool size, while minimizing scaling effects and staying within test recommendations from IMO (MSC, 2006). The model was built in a polyethylene foam (SIKA M150) and the hull was given an Epoxy coating, to give it a smooth surface. The model was provided with a shelf construction on top to allow for adjustment of the vertical center of gravity, and a wooden plank in the transverse direction to allow for adjustment of the moment of inertia, without affecting the center of gravity. Motions were measured with a 6-DOF motion censor, mounted close to the center of gravity. The model is seen in Fig. 2. The model should be able to test the influence of adding a bilge keel to the WTIV from a conceptual point of view, rather than a specific bilge keel. Therefore, the bilge keel was designed to be modular, such that it would be an easy adjustable add-on, which could be dismounted again. It was laser-cut in acrylic glass and mounted using three 3D-printed brackets on each bilge turn, which would be strapped to the hull. The bilge keel was designed with an angle of 45°, a breadth of 2.05 cm (1.74 m full scale) and a length of 97 cm (77.6 m full scale), i.e., a rather large bilge keel. The bilge keel is seen in Fig. 3. As a consequence of the modularity there was a small gap of 1.3 mm between the bilge turn and the bilge keel.

Before the actual roll tests, a number of preliminary tests were conducted to confirm the mass properties. A draught and trim check

[1] Global coordinate system has origin in the waterline and 4.2 m in front of the stern, in the transverse symmetry plane.

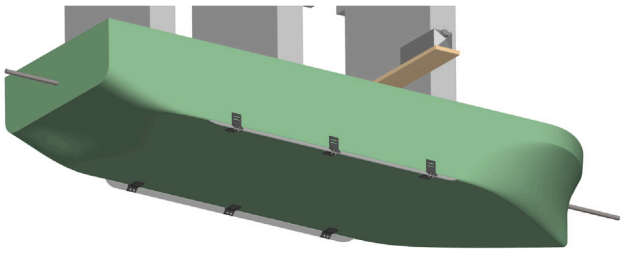

Fig. 3. CAD model of the experimental model with bilge keels, each bilge keel mounted with three brackets.

was performed to check the mass and the longitudinal and transverse position of the center of gravity. The trim and heel angles were obtained from draught marks and the motion sensor was used as a second reference. The vertical center of gravity was checked by conducting an inclination test. The heel angles were measured with the motion sensor and a pendulum as a second reference and was done for a variety of inclining moments to rule out uncertainties. From Eq. (6) the vertical center of gravity (z_G) can be obtained by recalling the restoring moment is a moment per unit of inclination $C_{44} = M/\phi$, assuming small angles for which $\tan(\phi) \approx \phi$.

$$C_{44} = \rho g \nabla (z_B - z_G) + \rho g \iint_{A_{WP}} y^2 \, ds = \rho g \nabla \overline{GM}_T, \tag{6}$$

where g is acceleration due to gravity, ∇ is displacement, z_B is vertical center of buoyancy (COB) and the integral term is the second moment of area of the water plane area. Roll period tests were conducted to check the moment of inertia. From Eq. (7) the roll period could be predicted and compared to the period measured experimentally, which would reveal any discrepancies in the moment of inertia.

$$T_{n4} = 2\pi \left(\frac{M r_{44}^2 + A_{44}}{\rho g \nabla \overline{GM}_T} \right)^{\frac{1}{2}}, \tag{7}$$

where M is the mass, r_{44} is the radius of gyration, and $\overline{GM}_T$ is the metacentric height. Having the mass properties established the roll decay tests could be conducted. The roll decay tests were initialized by pulling strings that were attached to the starboard side of the model and going through the pulleys, shown in Fig. 4. The motion sensor was connected live to a computer, from which the heel angle was monitored. To account for natural variation and to reduce the uncertainties each test was repeated three times. For all repetitive tests the strings were pulled until the same angle was obtained and then released by hand, once the model had stabilized. It was possible to release the roll motion within a heel angle tolerance of ±0.1°. The roll motion was observed until the amplitudes became insignificant, or the signal became dominated by drifting effects from the uncertainty of the sensor. First, free roll decay tests were conducted at different initial heel angles to investigate if the roll damping would be independent on the initial heel angle. Tests were conducted at the base loading condition at design draught in the initial heel range 2° to 11°.

Subsequently, the following roll decay tests were conducted:

- Free roll decay tests at varying vertical COG positions to investigate the influence of the COG on the roll damping. All tests were conducted at maximum draught, while the loading condition was changed between all the predefined loading conditions, shown in Table 2.
- Free roll decay tests with bilge keel at varying COG to investigate the difference of adding a bilge keel under different conditions. Tests were conducted under the exact same conditions as without bilge keel.

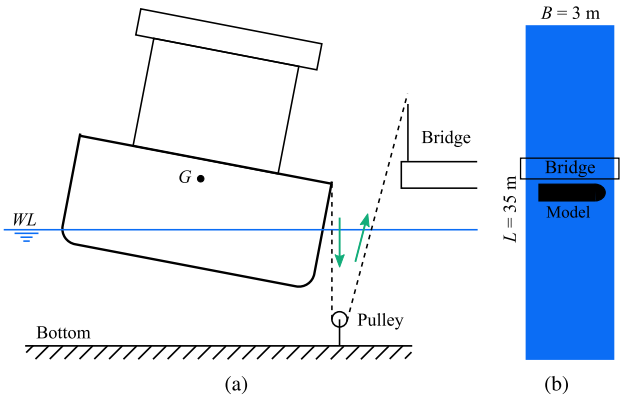

Fig. 4. Test setup. (a) Setup as seen from the side. (b) Basin layout, seen from above.

Table 2
Key parameters of dynamic mass properties of the six considered loading conditions, shown for both model scale (MS) and full scale (FS). Vertical COG (VCG) is given relative to the water line and the mass moment of inertia in roll, I_{xx}, is taken at the COG. Note that VCG and the inertia is non-dimensionalized for full scale according to Supplementary 3. Abbreviations: LC (loading condition), T (draught), HCOG1 (high COG condition 1), HCOG2 (high COG condition 2), LCOG1 (low COG condition 1), LCOG2 (low COG condition 2).

LC *Unit*	T [m]	VCG [MS/FS] [mm]/[–]	I_{xx} [MS/FS ($\times 10^{-2}$)] [kg m^2]/[–]
Base	5.5	203/0.332	7.88/2.962
Base	6.0	201/0.329	7.93/2.977
HCOG1	6.0	231/0.378	9.39/3.525
HCOG2	6.0	269/0.439	10.53/3.952
LCOG1	6.0	163/0.265	6.01/2.258
LCOG2	6.0	125/0.204	3.95/1.482

The first cycle of the roll is discarded to rule out transient effects of initializing the flow.[2] Data have been processed in a standardized way, according to Supplementary 1.A.

2.3. CFD modelling

The primary focus in the CFD modelling is firstly to create a model that is able to reliably predict the roll motion and roll damping at a high level of accuracy. The reliability is measured against the experimental results and therefore the model should be a replication of the experimental setup. Once the CFD model is validated in model scale, extracted damping coefficients can either be scaled directly through Eq. (4) or the entire CFD model can be scaled in space and simulations repeated. Both approaches are investigated. The CFD modelling have been done using the commercial software *STAR CCM+* (version 2022.1.1) and computations have been carried out at the HPC system *Niflheim*, located at *DTU Department of Physics*.

The model is based on the RANS equations and uses the k-ω SST (Menter) turbulence model (Siemens, 2022; Menter, 1994). The motion of the ship is modelled with the implemented dynamic fluid body interaction solver (DFBI), using the overset method to handle the motions of the vessel. Therefore the model consists of two regions: a background region and an overset region. The model uses the Multiphase Volume of Fluid model (VOF) cf. Hirt and Nichols (1981), and Siemens (2022) to model the interface between water and air. Walls are treated with blended wall functions based on Reichardt's law (*All y+*, Siemens (2022), Reichardt (1951)). The time integration uses a 2nd-order implicit temporal discretization scheme. The width and water

[2] Note that the last half part of the first cycle appears in the roll decay curves.

Table 3
Specification of boundary conditions in the numerical model.

Description	Boundary condition
Sides (basin walls)	Wall, no-slip
Outlet	Pressure outlet with wave damping
Bottom	Wall, no-slip
Top	Pressure outlet
Ship surface	Wall, no-slip
Overset boundary	Overset mesh

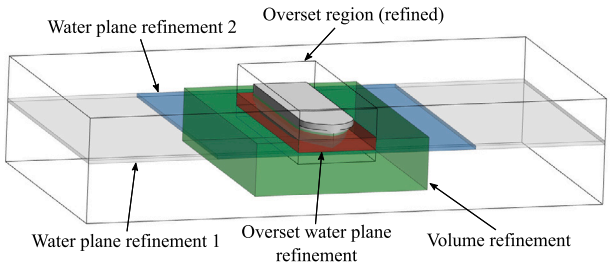

Fig. 5. Volumetric refinements: water plane refinement 1 (grey), water plane refinement 2 (blue), volume mesh refinement (green), overset waterplane refinement (red).

depth of the computational domain is the same as the experimental setup, but the domain length is limited to 6 meters to reduce computational time. The upper structure on the experimental model is not included in the CFD model, again to limit the computational time. The influence of drag on the structure from the air was investigated and found insignificant (not shown). Location of the COG, the mass and inertia properties are specified for the DFBI solver and all six DOFs are allowed. The equations of motion are solved in the center of gravity and non-diagonal components of the inertia matrix are assumed zero, meaning that the mass distribution of the ship alone does not introduce a coupling between the rotational modes. The boundary conditions in the numerical model are defined as shown in Table 3. At the outlets the pressure is specified as the hydrostatic pressure and with wave damping applied, which introduces resistance to vertical motion of the water, thereby damping the radiated waves in vicinity of the outlets to reduce wave reflections. The damping zone is specified to start 2.2 m from the boundary, corresponding to $0.8B$ from each of the sides of the ship, where B is the breadth.

The mesh is generated with a trimmer mesher which enables anisotropic meshing. Prismatic layers are used at all surfaces to resolve the viscous boundary layer, aiming at low y^+ values ($y^+ < 1$). Multiple volumetric refinements are used, each illustrated with a different colour in Fig. 5. The overset water plane refinement (red) is made higher to account for the rotation of the overset region. It is meshed isotropic with the same resolution as water plane refinement 2 has in z-direction, which in turn is meshed anisotropic.

The hull surface is refined using a surface control to have a target surface size of 50% of the base size of the overset region. Since the turns of the bilge are essential to the roll damping, it is of great importance to capture the flow correctly in these areas. Hence, the prismatic layers are gradually refined near the turns of the bilge by increasing the number of prismatic layers, from 10 and up to 25 layers, which is the result of a convergence study of the prismatic layers. A convergence study is performed, explained later in Section 3. The final mesh (after convergence study) is seen in Figs. 6 and 7 and the mesh configurations are presented in Table 4.

The bilge keel is modelled with minor changes from the experimental model to increase the numerical stability. The previously mentioned gap between the hull surface and the bilge keel on the experimental model is not modelled in CFD, as it is deemed to have minor influence, but would complicate the CFD modelling significantly. Additionally,

Table 4
Mesh parameters resulting from mesh convergence. '/' marks the sizes in refinements, from coarse to fine.

Region:	Background	Overset
Base size [mm]	30	15
Target surface size	50% base	50% base
No. of prism layers	5	10/15/25
Prism layer stretching	1.3	1.3
Prism layer thickness [mm]	4	4
Water plane cell size y [mm]	15/7.5	3.75
Water plane cell size z [mm]	50% of y	3.75

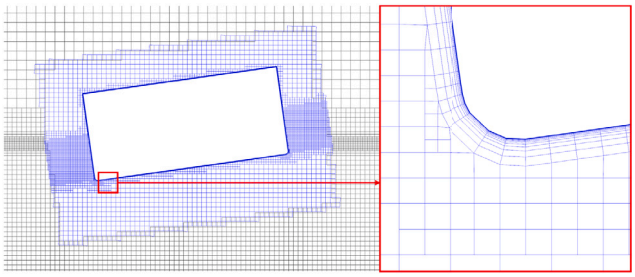

Fig. 6. Close-up on the overset region (left) and the prism layers (right).

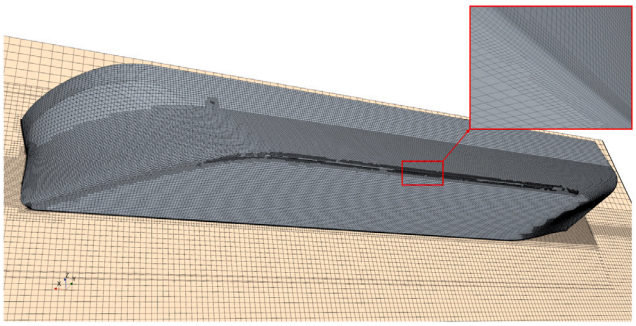

Fig. 7. Surface mesh and mesh of the longitudinal mid-section.

fillets are added to all edges, inner as well as outer (fillet radii 1.45 mm and 3.00 mm, respectively), to simplify the meshing in these areas and consequently the modelling of the flow. The influence of the fillets on the damping can be assumed negligible due to the bilge keel plate being thin relative to its breadth ($B/d = 5.125$). The bilge keel causes high flow velocities and severe flow separation at the edge of the bilge keel. Thus to resolve the flow near the bilge keel the mesh is refined in these areas, seen in Fig. 8, to 20% of the overset region base size (equating to an absolute cell size of 3 mm). Due to the high velocities and the fine mesh a smaller time step is required. Since the flow velocities change significantly during a roll cycle the bilge keel simulations use adaptive time step based on CFL conditions to reduce computational time, with minimum and maximum time step specified to 1.0 ms and 2.5 ms respectively. The CFL condition uses a target mean CFL number of 0.5 and a target maximum CFL number of 5.0.

The CFD model for simulating in full scale is much similar to that of model scale, though with a few alterations. The mesh is based on a scaled version of the mesh from model scale. Prismatic layers on the hull are adjusted to aim for high y^+ values ($y^+ > 30$) instead of low y^+ to avoid excessive computational time. The prismatic layers are refined more gradually in full scale, from 9 to 14 layers in 3 steps. Further, the relative total thickness of the prismatic layers is doubled in thickness to 0.64 m to get a smoother transition from the prismatic layers to the main mesh. The configuration of the prismatic layers is a result of a thorough analysis on a 10 m strip of the mid-ship cross section of the hull in full scale. It was found that the y^+ values fluctuates

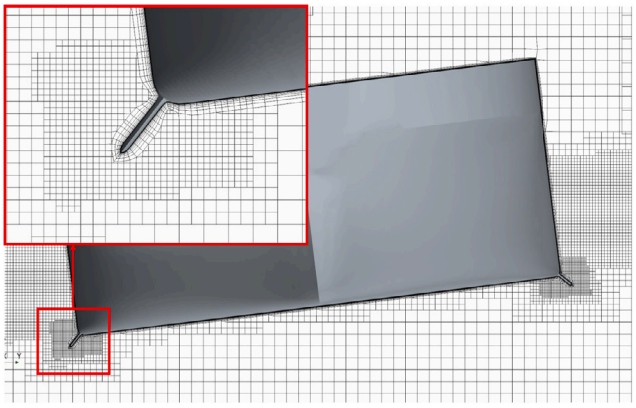

Fig. 8. Mid-ship section view of mesh with bilge keels.

significantly during a roll cycle due to the transient flow behaviour, making it difficult to configure prismatic layers to give reasonable y^+ values during entire roll decays and across several loading conditions. Thus, to test the influence of extreme y^+ values the 10 m strip was also modelled in a low y^+ configuration. The results should be similar for low y^+ and high y^+ if the solution is independent of extreme y^+ values. Since no experimental data is available in full scale the relative domain size and the wave damping zones are extended as a precaution to ensure that they will not influence the solution. The domain is extended from $\pm 4.9B$ to $\pm 10.2B$ corresponding to ± 500 m, and the wave damping zone was extended from $0.8B$ to $5.1B$, corresponding to 250 m, leaving $4.6B$ or 225 m between the ship and the start of the damping zone. For the damping zone to work sufficiently the damping zone should at minimum have a length of one wave length and to avoid influencing the motions it should be distanced minimum one wave length from the vessel, according to the recommendations of the VOF wave model from the manual of the software (*STAR CCM+*) (Siemens, 2022). The wave length can either be evaluated by measuring the wave length directly from a simulation or by estimating it from Eq. (8), assuming a regular gravity wave:

$$\lambda = \frac{g}{2\pi} T^2 \tanh\left(\frac{2\pi}{\lambda} h\right), \tag{8}$$

where λ is the wave length, T is the wave period (taken as the roll period), and h is the water depth. The degrees of freedom of the ship is limited to roll, heave and sway. To get closer to operating conditions the water was changed to salt water with a density of $1025\,\mathrm{kg/m^3}$ and a dynamic viscosity of 0.00114 Pa s. The full scale simulations use adaptive time stepping with the same CFL settings as in model scale, however with minimum and maximum time step specified as 4 ms and 20 ms respectively, which should be a conservative setting, as Froude scaling of the model scale settings would suggest 9 ms and 22 ms respectively.

3. Experimental and CFD results

3.1. Convergence study

The mesh presented in the previous section is the result of a convergence study. First, time step convergence is conducted on a very fine mesh (base size 20 mm). Using the converged time step, mesh convergence is studied with a base size ranging from 20 mm to 60 mm in steps of 10 mm. All cell sizes throughout the mesh, except the prismatic layers, are defined relative to the base size, thus the entire mesh is refined accordingly. Convergence of prismatic layers is studied separately. The convergence study is conducted for the loading condition with the lowest COG (LCOG2), as this is the most demanding case to simulate due to its high roll frequency. Convergence is evaluated firstly on the damping ratio, but also on the entire decay curve. Also CFL numbers and wall y^+ values are closely monitored. Only key results of the convergence study are presented here, and more detailed results can be found in Supplementary 2.A. Time step convergence is carried out using five different time steps and key results are presented in Table 5. It is seen that deviations of the damping, relative to the finest time step, is significant from time step 10 ms to 2.5 ms. At a time step size of 1.25 ms the deviation is down to −1.12% while the computational time becomes significant with a time step of 0.625 s. Therefore a time step of 1.25 ms is accepted and is used for the mesh convergence study. Key results of the mesh convergence study are presented in Table 6 where it is seen that the changes in damping are generally much smaller, but also more fluctuating than observed for the time convergence study. At a base size smaller than 30 mm the changes in damping are minor with only 1.52% deviation, but the additional computational cost is extensive. Hence, the solution is considered independent of the mesh when the base size is 30 mm, which is therefore used for all subsequent simulations. When scaling the mesh from full scale to model scale the convergence study should still be valid, provided that the prismatic layers have been studied exclusively. As a precaution, a simulation was performed with half the cell size of the scaled mesh (except prismatic layers, which was studied separately, as described in Section 2.3). No significant difference was observed, thus the convergence study from model scale is also valid in full scale.

Table 5
Time step convergence, evaluated on the roll damping of the second roll cycle, ζ_2, shown in percent of critical damping.

Time step [ms]:	10	5	2.5	1.25	0.625
ζ_2 [%]	3.32	4.18	5.08	5.28	5.34
Deviation [%]	−37.83	−21.72	−4.87	−1.12	–

Table 6
Mesh convergence, evaluated on the roll damping of the second roll cycle, ζ_2, shown in percent of critical damping.

Base size [mm]:	60	50	40	30	20
No. of cells [$\times 10^6$]	1.5	2.3	3.9	9.1	22.3
ζ_2 [%]	5.57	4.98	5.89	5.35	5.27
Deviation [%]	5.69	−5.50	11.76	1.52	–

3.2. Experimental and CFD model scale results

Prior to the experimental roll decay tests the mass properties of the model was verified through trim and draught tests, which is described in Supplementary 1.B. From the free decay tests at different initial heel angles it was found that for similar instantaneous roll amplitudes the roll damping is independent of the initial heel angle, provided that the first roll cycle is discarded. For further details, see Supplementary 1.C. Results from the free roll decay tests will be presented and discussed for the loading conditions with the highest and the lowest COG (loading conditions HCOG2 and LCOG2 respectively), and for the base loading condition at maximum draught, whereas the remaining loading conditions can be found in Supplementary 2.B. The decay curves are compared for the loading conditions HCOG2 and LCOG2 in Fig. 9(a) and for the base loading condition in Fig. 9(b). Note that the first half roll cycle is not shown. The CFD results are generally in good accordance with the experiments for all investigated loading conditions. The first four cycles fit very well, within the variation of the experimental test runs, after which the CFD results start to deviate from the experiments for all loading conditions, mostly in terms of period, but also amplitude and the deviations increase over time as the error accumulates. The deviation in period indicates a difference between the specified mass properties and the actual mass properties (mass, COG and inertia). The difference is relatively small though, as the deviations in period are only visible after some time, when

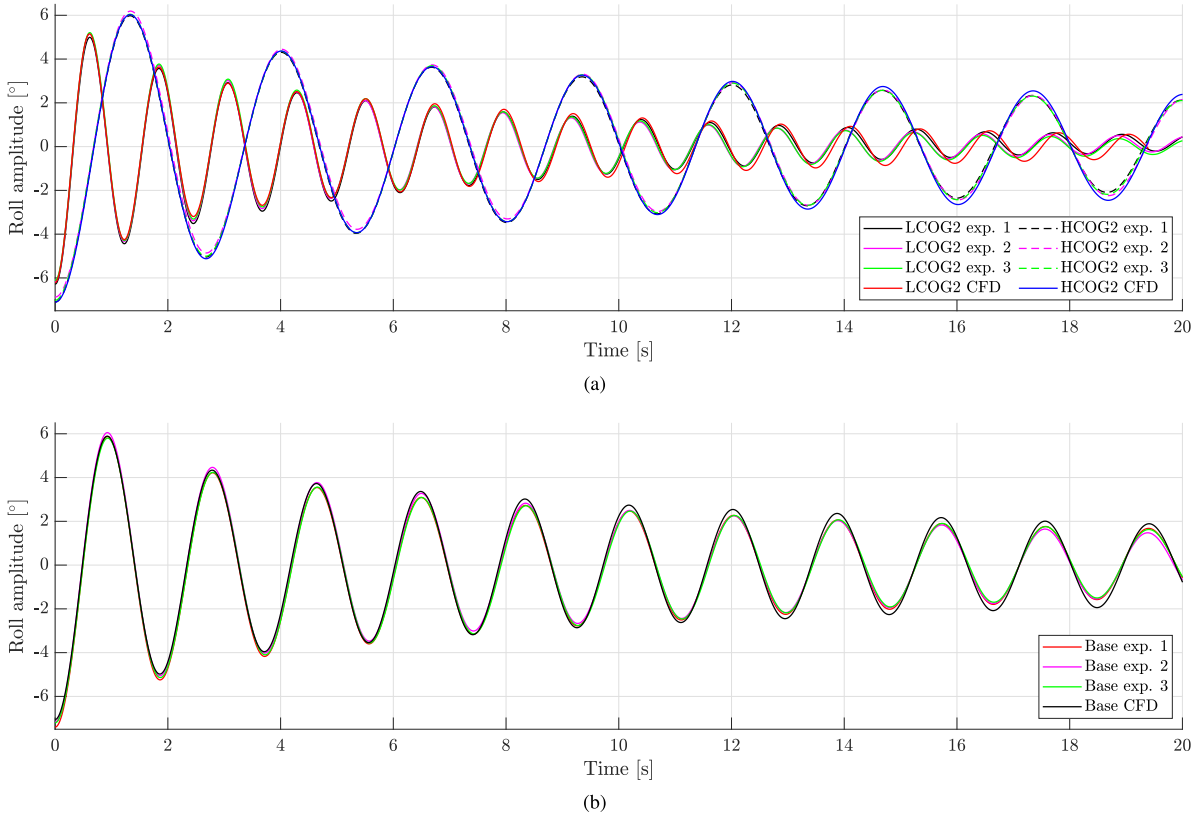

Fig. 9. Free roll decay curves for different loading conditions. (a) Highest and lowest center of gravity (HCOG2 and LCOG2), initialized from 8° heel angle and 7° heel angle, respectively. (b) Base loading condition at maximum draught, initialized from 8° heel angle.

Table 7
Experimental results of roll period (T_m) and number of cycles to cause 80 % reduction in the roll amplitude ($N_{80\%}$) relative to the initial heel angle, compared for different loading conditions (LC).

LC:	LCOG2	LCOG1	Base	HCOG1	HCOG2
T_m [s]	1.22	1.51	1.84	2.16	2.66
$N_{80\%}$	7.8	10.1	10.3	10.7	10.9

the errors have accumulated. Note that the roll period is significantly longer for high COG due to larger radius of gyration and smaller $\overline{GM}_T$. A comparison of the roll periods is seen in Table 7, along with the number of cycles to cause 80% reduction in the roll amplitude. It is seen that the loading conditions with high COG require more cycles, indicating smaller damping ratio.

In Fig. 10 the equivalent damping coefficient is shown as function of the roll amplitude where the experimental results are compared to CFD for the loading conditions LCOG2, Base and HCOG2. It is seen that the roll damping increases non-linearly with the roll amplitude. While the uncertainty is large for small roll angles, a weak tendency is observed of increasing damping ratios as the roll amplitude approaches zero. This increase might be explained by the KC number near the turn of the bilge becoming small (KC $\lesssim 1$), at which the flow regime may change from a turbulent separating flow towards a non-separating flow. Similar trends were observed by Sarpkaya (1986) who showed from experimental tests that the drag coefficient of a circular cylinder in a planar oscillatory flow increases as the KC number decreases (Faltinsen p. 238 Faltinsen, 1993; Sarpkaya, 1986). While the CFD results did not show any significant increase in damping at low roll amplitude, the CFD results did indicate a significant reduction in flow separations at low roll amplitudes. However, the uncertainty of the experimental results at such small roll angles ($< 2°$) is large, making it difficult to draw any solid conclusions on this tendency. From a practical point of view it is mainly the large roll motions that is of interest, as those are the limiting parameter defining how harsh weather the WTIVs can operate in. Thus, the large variation at small KC numbers is not considered problematic for the present study. By comparing the different loading conditions in Fig. 10 it is seen that the damping changes with the COG, where loading condition with low center of gravity has significantly larger damping than the others, confirmed by both experimental and CFD results. These observations, supported by the damping trend from Table 7, indicate that the roll damping becomes smaller for high centers of gravity. Furthermore, by comparing with the other loading conditions, e.g., base loading condition, it indicates that this transition is not linear, but that a certain threshold might exist, distinguishing at which vertical COG the damping will start to decrease significantly. Having knowledge of such a threshold could be useful in the design stages of vessels. As mentioned previously in Section 2.1, the damping for WSPCCs shows to subceed the predictions of Ikeda's Method and that WSPCCs share certain characteristics with WTIVs, such as shallow draught, wide breadth and high COG. The WSPCC investigated by Kawahara et al. (2011) had a $COG/d = -1.35$ whereas the loading conditions LCOG2 and LCOG1 has $COG/d = -1.67$ and $COG/d = -2.17$, respectively.[3] Thus the relative COG investigated in the present study is significantly higher than the WSPCC. A parameter that may influence is the breadth-to-draught ratio, which for the WSPCC is $B/d = 4.90$ and for the investigated WTIV is $B/d = 8.17$. Thus, the characteristics are similar compared to conventional ships, though they are more distinctive for the WTIV. Hence Kawahara's findings (Kawahara et al., 2011) contributes to the validity of the observed damping behaviour at LCOG2. Since all the investigated loading conditions still have relatively high COG, compared to conventional ships, it could

[3] Note that the COG is defined negatively in this parameter, when above the water line.

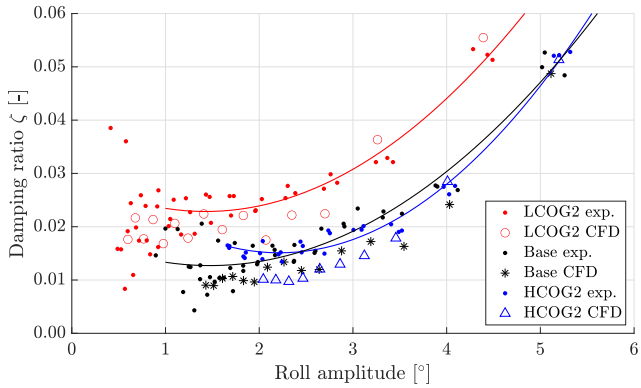

Fig. 10. Equivalent damping as function of roll amplitude. Results from all three experimental test runs are shown, along with the CFD results. The base loading condition is at maximum draught. The solid lines are polynomial fits to the experimental data, to illustrate the trends.

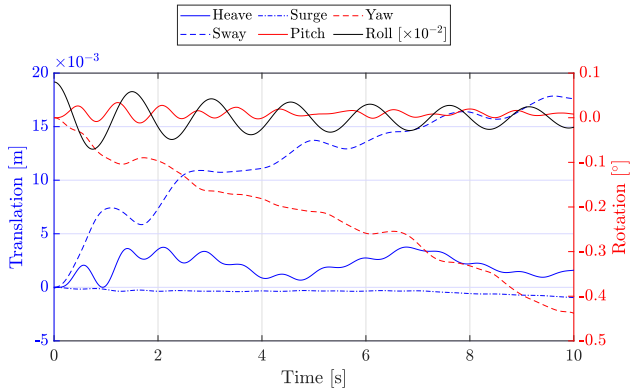

Fig. 11. Motion in all six degrees of freedom for the loading condition with low COG (LCOG1).

be interesting to investigate a much wider range of COG and across different vessel types, but this is beyond the scope of the present paper.

In Fig. 11 all 6 degrees of freedom are compared in a double plot. It is seen that sway and yaw represents the largest motions besides roll, which is in line with the expectation, because they are coupled with roll. However, compared to roll their motions are insignificant, indicating that it is a fair assumption to consider the roll decay as a 1-DOF motion. The motions generally behave as expected.

3.3. Bilge keel — experimental and CFD model scale

In Figs. 12(a) and 12(b), the decay curves from experiments and CFD with bilge keel are compared for the loading conditions HCOG2 and LCOG2, respectively. The damping ratios are compared in Fig. 13. From the decay curves in Fig. 12 it is seen that the CFD is able to reproduce the experiments to a high precision for both the loading condition with high COG and the loading condition with low COG, but the loading condition with low COG deviates slightly more in amplitude, which is also reflected in the damping ratios in Fig. 13. From the loading condition with low COG it is observed that the damping ratios from CFD is fluctuating, both for the bare hull and with bilge keel. It is estimated that the uncertainty of the CFD is the amplitude of the fluctuations. Compared to the results of the bare hull it is clear that the bilge keels change the roll decay quite significantly. The number of roll cycles to cause 80% reduction in the roll amplitude is more than halved, from 8 to 3 cycles, seen in Table 8. It is also noted that the period is increased with approximately 0.05 s for all loading conditions. The increase in period is expected to be due to increased

Table 8
Experimental results of roll period (T_m) and number of cycles to cause 80% reduction in the roll amplitude ($N_{80\%}$) relative to the initial heel angle, compared for different loading conditions (LC) with bilge keels.

LC:	LCOG2	LCOG1	Base	HCOG1	HCOG2
T_m [s]	1.26	1.56	1.89	2.21	2.71
$N_{80\%}$	2.6	3.0	3.1	3.0	3.0

added mass after the bilge keel is added. From Fig. 13 it is seen that the damping ratio is increased significantly, and moreover the steepness of the damping is increased, thus it has a stronger dependence on the roll amplitude, resulting in much larger maximum values. On the discussion of the dependency of the damping on COG, it is seen from Fig. 13 that the relative difference between the loading conditions appears smaller with the bilge keel but the absolute difference is in the same order of magnitude, slightly smaller. Due to the large uncertainty at small amplitudes the damping ratios in this region should be used with great care.

In Fig. 14 the development in flow during a roll cycle is shown in the mid-section of the ship for the bare hull and with bilge keels. For the bare hull (left) it is seen how eddies are formed on the down-stream side of the turn of the bilge, and at some point during the roll are released from the ship and continues as a vortex in the near-area. In Fig. 15 the vorticity during a roll cycle is shown, where it is clearly seen from the bottom right picture how a vortex is formed on the downstream side of each bilge keel. Similar to many other problems in ocean engineering (Gao et al., 2019; Shao et al., 2019; Ding et al., 2022; Lei et al., 2023), the generation, advection and diffusion of the vorticities change the pressure distribution on the structure, and thus may provide significant viscous damping.

3.4. CFD full scale results

Full scale simulations are performed for the loading conditions with the highest and lowest center of gravity, HCOG2 and LCOG2, and for the base loading condition at maximum draught. The resulting decay curves are seen in Figs. 16(a) and 16(b) respectively and their damping ratios are compared in Fig. 17. Comparing full scale and model scale, Figs. 16 and 9 respectively, it is seen that full scale remains at higher amplitudes for much longer time, across all investigated loading conditions indicating that the damping is smaller. From the damping ratios in Fig. 17 it is generally seen that the damping is much smaller in full scale, but also the difference in damping between the loading conditions is more significant. Due to the much smaller damping the roll decays does not cover the same range of amplitudes, as it would require considerably longer simulation time to reach the same amplitudes in full scale. The loading conditions with high COGs in full scale generally have a very small damping, especially for amplitudes smaller than 5°. The much smaller damping in full scale indicates that the viscous scaling effects in model scale are significant. To investigate this, the Reynolds number has been estimated for the base loading condition in model scale and full scale, presented in Table 9. It is seen that the Reynolds number is much smaller in model scale, indicating that the damping in model scale is dominated by viscous (laminar) flow, whereas in full scale, where the flow is more turbulent, the influence of the viscosity is smaller. The free surface of the full scale base loading condition is shown in Fig. 18, where it is seen that the waves has dissipated before they reach the boundaries, thus no sign of any wave reflections. The distance between the wave crests have been measured to be approximately 97 meters. Alternatively the wave length could be calculated from Eq. (8), which would yield 389 m, thus too long compared to the measured length of 97 m. This could indicate that the radiated waves are not continuous gravity waves but rather abrupt waves generated over a short amount of time, which also explains that the free surface elevation in Fig. 18 is not symmetric about calm water level ($z = 0$ m).

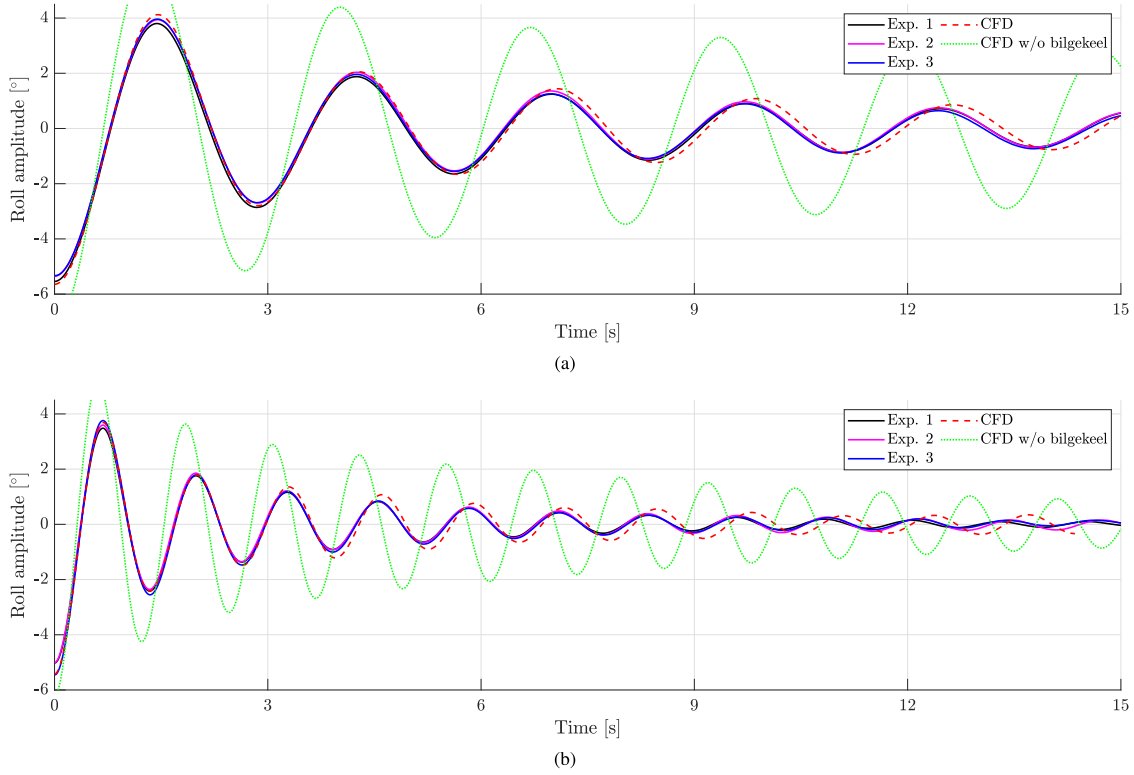

Fig. 12. Free roll decay curves for different loading conditions with bilge keels, both initialized from 7° heel angle. (a) Condition with the highest center of gravity (HCOG2). (b) Condition with the lowest center of gravity (LCOG2).

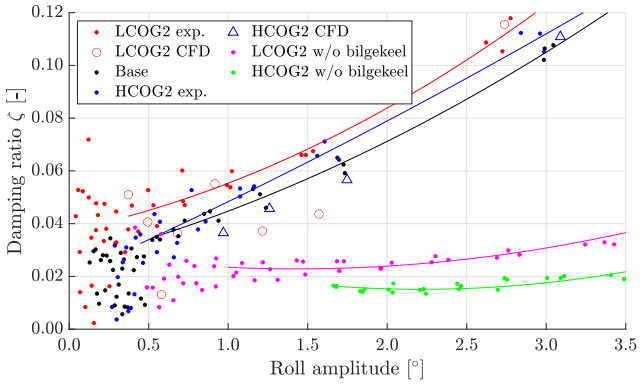

Fig. 13. Experimental damping ratio for different loading conditions with bilge keel, compared with CFD, and with experimental result from bare hull. Note that trendlines are polynomial fits based on experimental data.

Table 9
Reynolds number for the base loading condition, calculated at the turn of the bilge with the peak angular velocity during the second roll cycle. The characteristic length is taken as the roll radius to the bilge (i.e., distance from COG to the turn of the bilge).

	Model scale	Full scale
Roll period [s]	1.86	16.20
Peak angular vel., ω_2 [rad/s]	0.274	0.040
Characteristic length [m]	0.417	33.356
Reynolds number [–]	4.519×10^4	3.956×10^7

3.5. Quadratic damping

From the experimental or CFD results non-linear damping coefficients may be extracted for later use in a potential flow solver. The loading condition with low COG (LCOG1) in model scale is used as a show case example. Quadratic coefficients are extracted by using the procedure outlined by Faltinsen (1993), explained in Section 2.1, from which the damping is expressed as $\frac{1}{T_{n4}} \log\left(\frac{\phi_{i-1}}{\phi_{i+1}}\right)$ and the mean amplitude is expressed as $\frac{16}{3}\frac{\phi_i}{T_{n4}}$. A linear function is fitted to the data which gives the linear and quadratic damping coefficients. For using a cubic damping model the same procedure is applied, but fitted with a second order polynomial. In Fig. 19 different fittings are shown. Note that the curve "Linear fit, b_2" is forced through origin, hence $b_1 = 0$. Many commercial seakeeping softwares have user-specified quadratic damping implemented as an option, but often only the quadratic term can be specified. The linear term, which mainly represents the wave radiation, is calculated from potential flow theory. Applying a b_2 value without the related b_1 has however shown to give inaccurate results, as the b_1 calculated from potential flow deviated significantly from that obtained from fitting the experimental data. Hence if only a quadratic coefficient can be specified, the linear fit should be forced through origin. To investigate the consequence of this approximation, both cases have been included. From Fig. 19 it is seen that the cubic model has the best fit, as one might expect. The damping coefficients are presented in Table 10, along with the error R^2. Note that the linear damping is simply the mean of the observed damping ratios. From Table 10 it is seen that the cubic model presents by far the best fit and that both of the quadratic models are quite similar to each other in terms of the error. The quadratic damping coefficient b_2 has been calculated for all the investigated loading conditions, presented in Table 11. It is seen that the quadratic coefficients for bilge keel is approximately five times higher than without bilge keel. As seen from the error some of the fits are quite poor while others, such as the bilge keel with high COG (HCOG2), is fitted to a high precision. It is found that the cubic damping models are much better fitted to the data with R^2 close to 1 for all cases. Before the damping coefficients can be applied in a motion analysis they must be dimensionalized using Eq. (4).

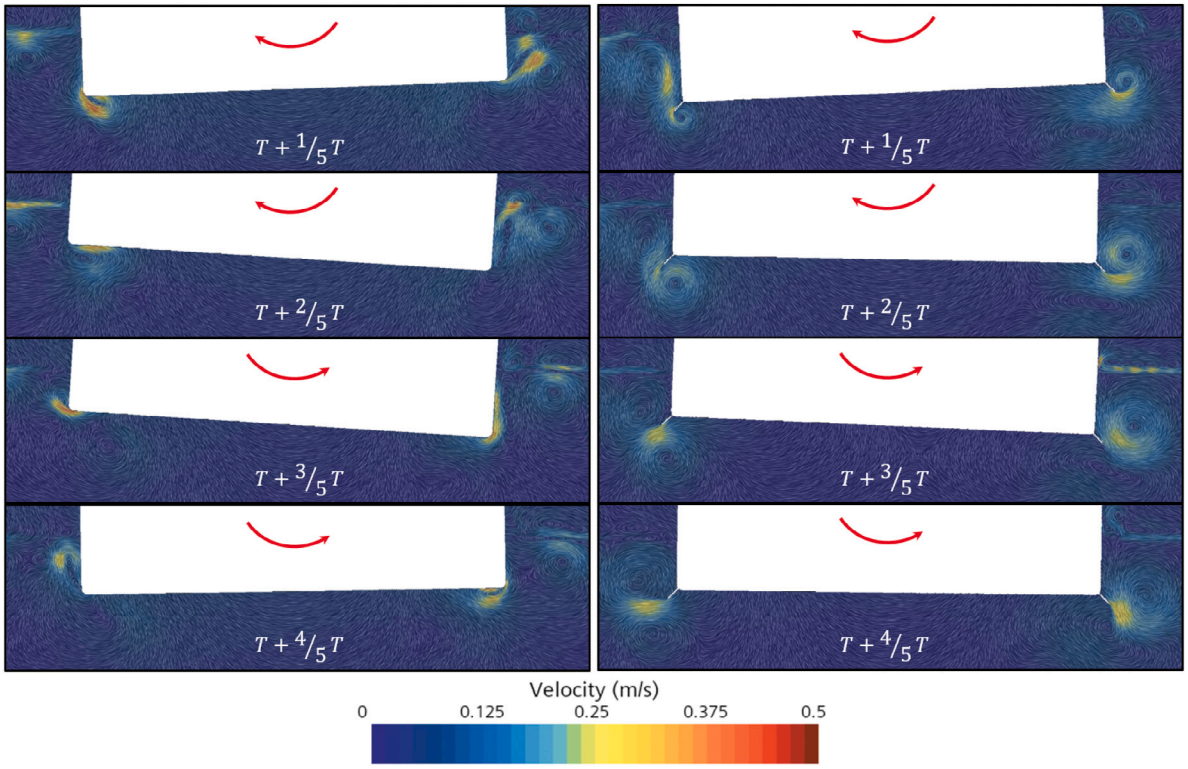

Fig. 14. Development in flow velocity during one roll cycle for the bare hull (left) and with bilge keels (right) from CFD model scale. Time is indicated with the roll period T.

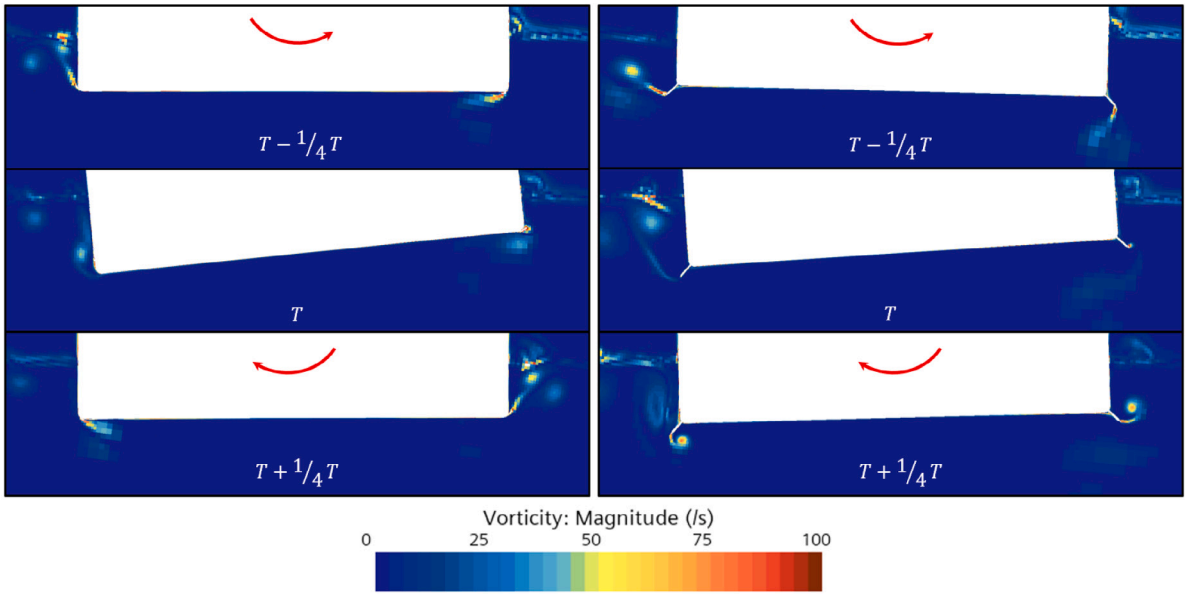

Fig. 15. Vorticity during a roll cycle for the bare hull (left) and with bilge keels (right) from CFD model scale. Time is indicated with the roll period T.

Table 10
Non-dimensional damping coefficients with error estimate for different orders of damping model, obtained from CFD model scale data of the loading condition with low center of gravity, LCOG1.

Damping model	b_3	b_2	b_1	Error, R^2
Linear	–	–	0.132	–
Quadratic, b_2	–	1.062	0	0.830
Quadratic, b_2, b_1	–	1.391	−0.059	0.888
Cubic	5.848	−0.830	0.121	0.959

Similar to model scale, damping coefficients are extracted from full scale results using the same procedure. The base loading condition at maximum draught is used as a show case example, for which the polynomial fitting is seen in Fig. 20 and the resulting damping coefficients are presented in Table 12, where it is seen that the damping coefficients are generally smaller, as expected. Quadratic damping coefficients from the other investigated loading conditions are presented in Table 13. Note from the R^2 errors that some of the fits are quite poor, which is caused by a combination of the damping not fitting well to a linear function and the fitting being forced through origin, of which the latter is especially the case for the loading condition with low COG. From

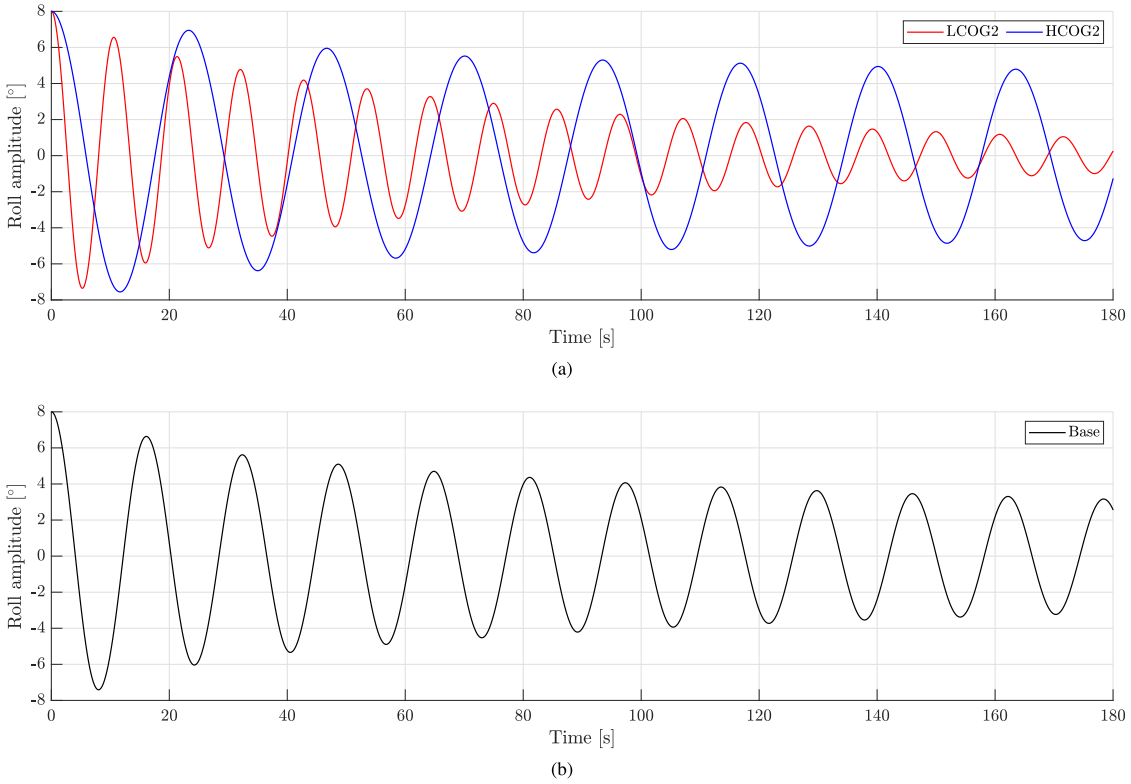

Fig. 16. Free roll decay curves for different loading conditions. (a) Condition with the highest center of gravity (HCOG2), initialized from 8° heel angle. (b) Condition with the lowest center of gravity (LCOG2), initialized from 7° heel angle.

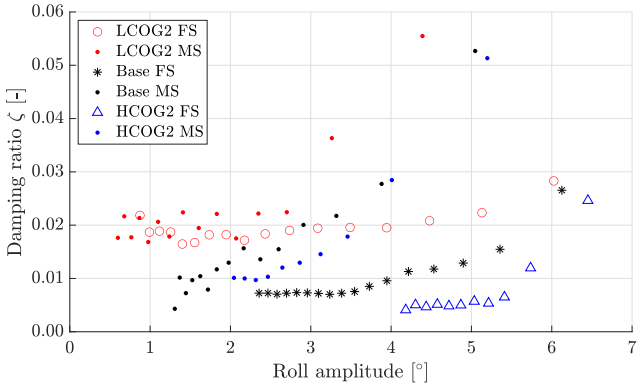

Fig. 17. Equivalent damping as function of roll amplitude. Results are shown for one experimental test run for each of the loading conditions, along with the full scale CFD results.

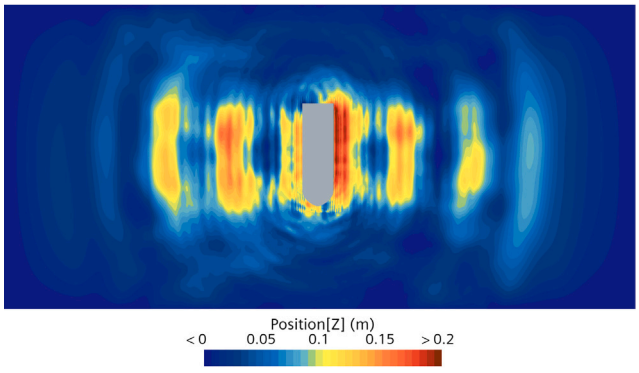

Fig. 18. Free surface elevation from the base loading condition, taken after 195 s of decay.

Table 11
Non-dimensional quadratic damping coefficients (b_2) along with the respective errors (R^2) for different loading conditions, all at maximum draught 6 m, obtained from model scale. Note that the damping coefficients for bilge keel are based on roll angles larger than 0.5°. Abbreviations: LC (loading condition).

LC	LCOG2	LCOG1	Base	HCOG1	HCOG2
b_2 [–]	1.671[a]	1.062	1.008[a]	0.877	1.033[a]
R^2	0.500	0.830	0.818	0.611	0.769
With bilge keel:					
b_2 [–]	6.226[a]	5.283[a]	5.050[a]	4.978[a]	5.627[a]
R^2	0.586	0.448	0.857	0.923	0.971

[a] Marks that it is extracted from experimental data.

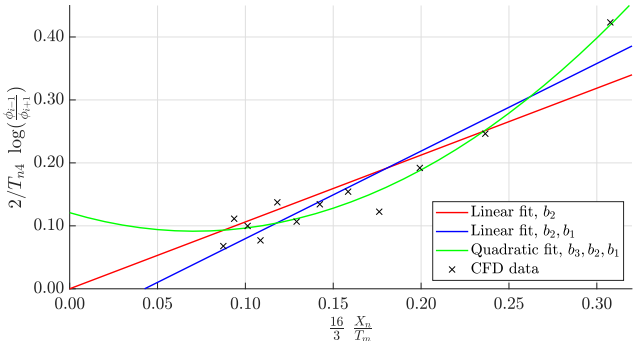

Fig. 19. Polynomial fitting of different orders in the least square sense on model scale CFD data of the loading condition with low center of gravity, LCOG1.

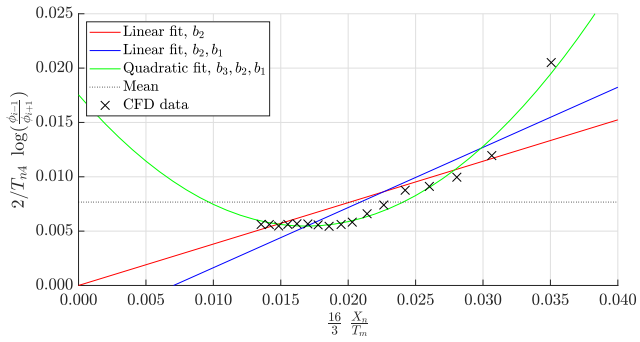

Fig. 20. Polynomial fitting of different orders in the least square sense on full scale CFD data of the base loading condition.

Table 12
Non-dimensional damping coefficients with error estimate for different orders of damping model, obtained from CFD full scale data of the base loading condition at maximum draught.

Damping model	b_3	b_2	b_1	Error, R^2
Linear	–	–	0.008	–
Quadratic, b_2	–	0.381	0	0.708
Quadratic, b_2, b_1	–	0.554	−0.004	0.791
Cubic	42.489	−1.433	0.018	0.975

Table 13
Non-dimensional quadratic damping coefficients (b_2) along with the respective errors (R^2) for different loading conditions, all at maximum draught 6 m, obtained from full scale.

LC	LCOG2	Base	HCOG2
b_2 [–]	0.804	0.381	0.217
R^2	−8.460	0.708	0.269

Fig. 20 it is seen that the linear fits (i.e., quadratic damping) do not fit the shape of the data well and are too simple, which will results in significant underestimation of the damping at large roll amplitudes. The quadratic fit however (i.e., cubic damping) fits well within the existing data, but increases excessively for smaller amplitudes. Considering linear damping it is clear that this is a poor fit. The damping might be close to linear for small amplitudes but not for large amplitudes, thus a linear damping model will overestimate the damping at small amplitudes and underestimate the damping at large amplitudes. Generally this section shows that it may not be reasonable to fit to an entire decay curve, which is also remarked by Faltinsen (1993). Instead, a piece-wise damping function might be more appropriate, where different quadratic coefficients are applied dependent on the range of amplitudes.

4. Application and discussion

4.1. Roll motion in an irregular beam sea with and without bilge keels

By applying the previously obtained damping values in a hydrodynamic motion study maximum roll angles are calculated considering different combinations of sea states and damping models. The most common options for applying roll damping in commercial software are Ikeda's method, user-specified linear damping or quadratic damping. The performance of these models is compared and discussed. The hydrodynamic motion study is conducted with the panel method based commercial software WADAM, provided by DNV (SESAM, 2021). The ship is modelled in full scale under the loading condition LCOG1. The sea state is defined with the JONSWAP wave spectrum with a significant wave height of 3.5 m and zero-upcrossing periods ranging from 6.5 s to 19 s. The vessel is subjected to beam-sea condition, i.e. waves propagate along the transverse direction of the ship. The analysis is based on short term statistics with a duration of 10 800 s (three hours). Roll damping using Ikeda's method is also calculated, using a strip method for which the ship is descritized into 14 strips, each 10 m long. The following damping models are investigated:

- Roll damping model, conventional (Ikeda's method).
- Roll damping model, barge (Ikeda-based, ITTC 2011, barge (ITTC Specialist Committee et al., 2011)).
- Global quadratic damping (extracted from model tests).
- Linear damping matrix (10% critical damping).

As the bilge keel is only simulated in model scale quadratic coefficients are consistently extracted from model scale in order to have a relative comparison. The linear 10% critical damping is included as this is not an uncommon assumption in the lack of experimental data. The Ikeda damping is calculated in WADAM, in which damping models are specified to assume turbulent flow and apply stochastic linearization.

As a fast and convenient way of checking the damping coefficients before they are used for further motion studies, they are inserted into a 1-DOF equation of the form stated in Eq. (1) and is given an initial heel angle, similar to that of the CFD model, with no external force applied. The equation is solved in the time domain using an ordinary differential equation solver, thus a free roll decay motion is obtained. Added mass, restoring and damping coefficients are determined in WADAM, calculated at a wave frequency coinciding with the natural frequency (e.g. the free decay roll frequency). The resulting decay curves are compared in Fig. 21. The decay curve resulting from Ikeda's damping uses the equivalent linear damping, calculated from WADAM at the roll natural frequency. From Fig. 21, it is seen that the quadratic model is in good agreement with the CFD during the entire decay period though with slight deviations in period, which accumulates over time. This indicates that the coefficients are correct. The cubic model is very similar, though it actually dampens too much during the first three cycles, making the quadratic model a better fit. Ikeda's damping overestimates the amplitude in the beginning and then underestimates later with significant deviations after 10–12 s. From the linear 10% critical damping, it is clear that the damping is too high and the decay curve deviates significantly from the CFD. After 10 s no roll is left, while in reality the ship is still rolling with ±2°. Thus, it is a poor assumption to use 10 % critical damping for this particular case. The difference between quadratic damping using both coefficients, b_1 and b_2, and using only b_2 has been investigated (not shown), which showed that the difference is vanishingly small, thus the benefit of using both coefficients is insignificant. With the damping coefficients validated, they can safely be used in the motion study in WADAM.

From WADAM the transfer functions (RAOs) are obtained for each sea state. Combined with the wave spectra through Eq. (9), the response spectra are calculated as

$$S_R(\omega) = S_\zeta(\omega)|\Phi_R(\omega)|^2, \tag{9}$$

where S_ζ is the wave spectrum and Φ_R is the transfer function. Note that while transfer functions usually are assumed independent of sea state (wave spectrum), this is not the case for roll if a viscous damping model is used. This is because the roll damping is dependent on the roll amplitude which in turn is dependent on the exciting waves, hence the sea state. This interdependency is solved through an iterative procedure. Therefore, the transfer function is influenced by the wave spectrum and should only be used in this combination of sea state. Extreme values of the roll angle can then be predicted from short term statistics. It is assumed that the sea state is a stationary process, and that the peaks of the roll amplitudes, e.g., in a time realization of the response spectrum, will follow a Rayleigh distribution. From the response spectrum the standard deviation and the zero-upcrossing rate is calculated, which is used to calculate the extreme value of the roll amplitude from Eq. (10).

$$\tilde{\mu}_q = \sigma_X \sqrt{2 \ln\left(\frac{N_z}{\ln \frac{1}{1-q}}\right)}, \tag{10}$$

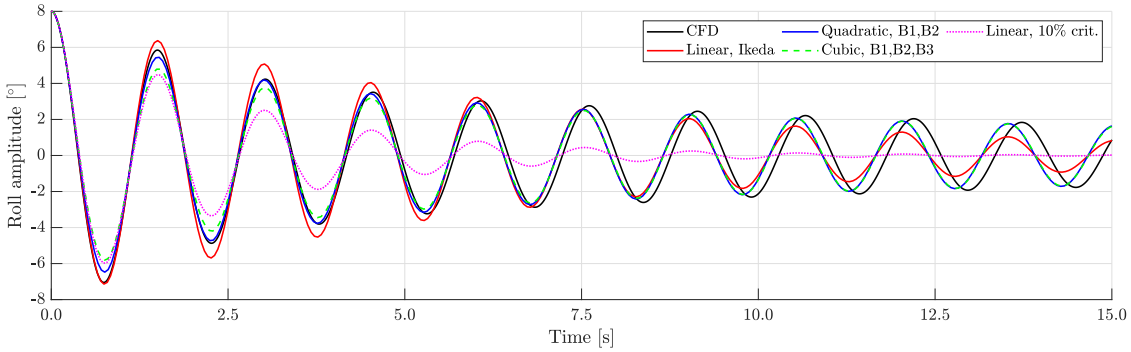

Fig. 21. Comparison of CFD and 1-DOF solver with different damping models.

Table 14
Reduction in roll angle with bilge keels for different T_z, given in percent based on the results from quadratic roll damping.

T_z [s]	6.5	8	11	12	13	15	17	19
Reduced [%]	19	38	45	42	39	39	38	38

Here q is the probability fractile in the Rayleigh distribution, N_z is the number of zero-upcrossings during the time duration of the short term analysis, and σ_X is the standard deviation of the response spectrum. Using $q = 0.5$ the extreme values are calculated for the different sea states and damping models, and results are presented in Fig. 22. From Fig. 22(a) it is seen that the quadratic model predicts the largest motions, which peaks close to the natural frequency. Ikeda's damping is in good accordance with the quadratic model at high T_z values, but in poor agreement for $T_z < 12$ s. The barge model predicts significantly smaller motions than both the Ikeda and the quadratic model, which is unfortunate, as it seems like an obvious choice of damping model due to the shared vessel characteristics. As expected the 10% critical damping predicts too small motions because the damping is too large and over-simplified. For $T_z \leq 8$ s the difference between the damping models, except the quadratic, is small, which is caused by the transfer function and the wave spectrum having only a small overlap, at which the influence of the damping model is insignificant. The quadratic results are considered as the most reliable, since the damping is extracted directly from CFD, confirmed by experimental tests and finally validated in a 1-DOF motion solver. However, it should be noted that motions from quadratic damping is influenced by the linear data fitting, which underestimated roll damping at large amplitudes. Further, the damping has not been investigated at roll amplitudes above 8°. Thus, the resulting roll angles from quadratic damping is expected to be overestimated, but is still considered the most accurate of the applied methods. Comparing this with Fig. 22(b) it is clear that the motions across all damping models are significantly smaller with the bilge keel added. Percentwise reductions of roll motion with the bilge keel are shown in Table 14. The largest reduction is observed close to the resonance frequency at 11 s where the roll amplitude is reduced with 45%.

4.2. Roll motion in an irregular beam sea using full scale derived damping

In this section extreme values of the roll motions has been calculated, similar to previous section, but using damping coefficients derived from full scale simulations. This is done on the base loading condition at maximum draught, as this is likely to be the most common loading condition for the vessel fully loaded with wind turbines. The sea state was defined as a JONSWAP wave spectrum with a significant wave height of 3.5 m and zero-upcrossing period ranging from 6.5 s to 19 s and waves coming in from the side (beam sea). As for the previous section, the full scale damping coefficients has been pre-checked in a

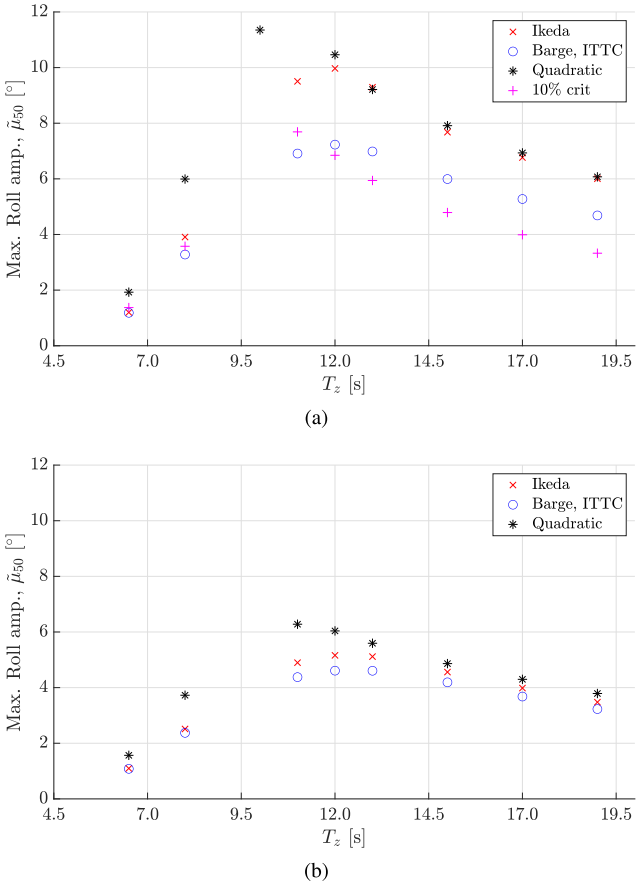

Fig. 22. Extreme value with 50% fractile from short term statistics using a significant wave height $Hs = 3.5$ m and different T_z for the loading condition with low COG, LCOG1, using model scale damping data. (a) Bare hull. (b) With bilgekeel.

1-DOF motion solver, seen in Fig. 23, before they are applied with a sea state in WADAM. It is seen that the quadratic and cubic damping models are replicating the CFD decay to a high accuracy, while both linear models are deviating considerably. Thus, the quadratic damping model is well suited, provided that the roll amplitudes from a motion study are within the range of investigated amplitudes ($\lesssim$8°). Extreme values from the different damping models are calculated and are seen in Fig. 24. The linear damping model (derived from CFD) yields exaggerated roll motions with amplitudes larger than 20° near the resonance frequency which is far beyond the range of amplitudes that the damping has been investigated for. The quadratic damping model also yields rather large motions up to approximately 15° near the resonance frequency, which is also considerably above the investigated range of amplitudes. On the

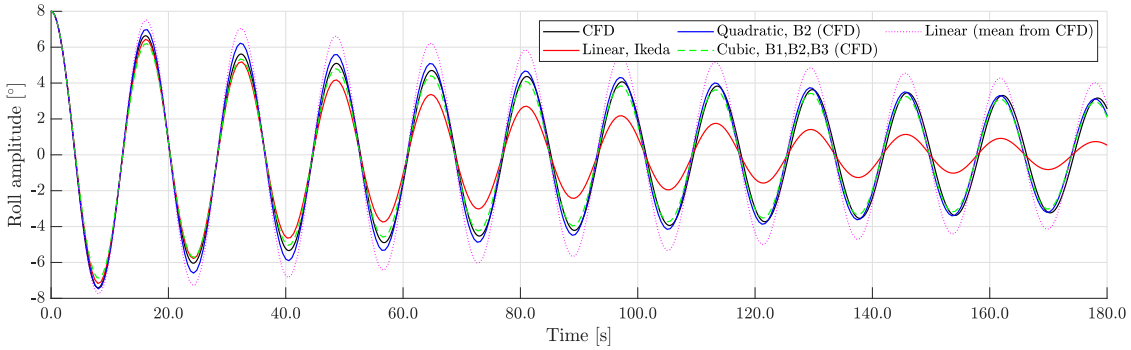

Fig. 23. Comparison of CFD and 1-DOF solver with different damping models for base loading condition in full scale.

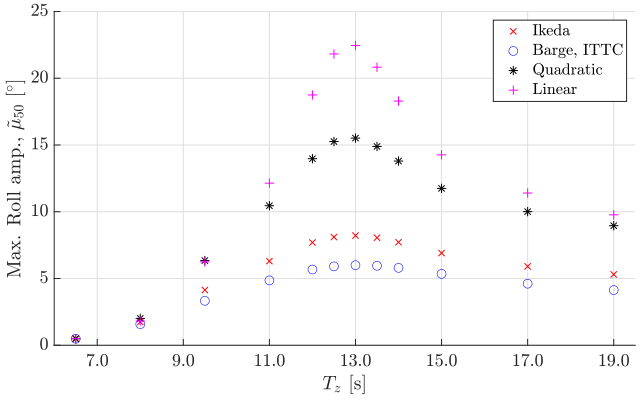

Fig. 24. Extreme value with 50% fractile from short term statistics for different T_z for the loading condition with low COG, LCOG1, using model scale damping data.

other hand the Ikeda-based damping and the barge model yields much smaller motions, up to 8° and 6° respectively, which is similar but slightly smaller than the motions from the loading condition LCOG1. It is expected that the motions in reality would be somewhere between the results of the Ikeda-based damping and the quadratic damping, as the quadratic model in this case underestimates the damping for large amplitudes.

4.3. Final discussions

On the discussion on the choice of damping model, the extreme value predictions showed that Ikeda's method strongly overestimate the roll damping, causing too small predictions of motions, when benchmarked against full scale derived quadratic damping. As the data fitting for extraction of the quadratic coefficients was dominated by small roll amplitude data, the full scale based quadratic damping underestimated the roll damping at large amplitudes. Hence the Ikeda's method may not overestimate as strongly as the figures may suggest (e.g., Fig. 24), however it is still expected to overestimate significantly. The ITTC 2011 barge model was found to overestimate the roll damping significantly, regardless if it is compared with model scale or full scale derived quadratic damping. Originally the barge model was developed as a simplified formula to add more viscous roll damping, because it had been shown that Ikeda's method underestimated the eddy roll damping for barges. This means that while Ikeda's method already overestimates the damping, the barge model adds even more damping, making the extreme value predictions significantly smaller. The significant scaling effects from full scale to model scale is remarkable as scaling effects in roll according to ITTC 2011 (ITTC Specialist Committee et al., 2011) for a 2 m long model usually only accounts for 8%–10% (unspecified ship type). The extreme value prediction with quadratic damping can be questioned by being purely based on measurements conducted at the natural frequency. It could be advantageous to use the CFD model to perform forced roll tests at other frequencies to investigate this influence. However, since the largest roll angles are observed close to the natural period, the quadratic damping should be valid for this frequency. Full scale measurements from a ship in operation in a beam sea would be valuable as a third reference.

From this discussion today's state of the art, i.e. the recommendations of ITTC 2011, does not seem suitable for the considered WTIV, as this study have shown that they are not conservative. As this study was designed with a basis in the North Sea the likelihood of waves coinciding with the natural frequency seems small as zero-upcrossing periods larger than 8.5 s is rare, based on scatter diagrams. Increasing the vertical COG will further reduce the likelihood. Considering other locations such as the east coast of North America such conditions are more common, making the discussion particular relevant, hence nothing general can be concluded from this as the operational conditions are site-specific. Note that the results from Fig. 22 cannot be linearly scaled with the wave height because of the interdependency between the non-linear damping and the roll amplitude.

The investigated bilge keel reduced the extreme value predictions significantly, though mostly at large T_z values. The investigated bilge keel was large compared to normal bilge keels, however similar sizes are seen on FPSO vessels. While this study cannot fully justify the use of bilge keels on WTIVs, it has however shown the potential benefits, hence justifying a deeper investigation on the topic to cover both the hydrodynamic potentials as well as implications on other matters, such as operation and hull construction. Considering the forecasts in offshore wind and the increased demand of WTIVs the presence of bilge keels on this vessel type is not a distant thought. The study have also shown that CFD can be beneficial in the design stage of bilge keels to accurately quantify a design.

5. Conclusions

A CFD model has been developed as a digital twin to predict roll damping through free decay tests of a Wind Turbine Installation Vessel (WTIV). It is validated through experimental tests, which showed that the CFD model was fairly accurate, with average deviations in damping ranging from −4.6 % to 14.2 % for large roll amplitudes (>3°), depending on the loading condition.

It was shown that the roll damping increases for a low COG, thus indicating that WTIVs have relatively small roll damping due to their high COG. Simulations in full scale showed that the damping is significantly smaller than that in model scale, with reductions ranging from 62% to 90% for large roll amplitudes (>5°), depending on the loading condition. The largest deviations were observed at loading conditions with high COG.

Quadratic roll damping was found as an appropriate damping model, though it may not be suitable for a wider range of roll angles. A

piecewise damping approach is suggested. Extracted quadratic coefficients were applied in a seakeeping analysis. Ikeda's method was found to overestimate the roll damping slightly when compared to model scale and significantly when compared to full scale, especially for small zero-upcrossing periods (T_z). The ITTC barge model significantly overestimated the roll damping, resulting in too small roll angles and is concluded inappropriate for the considered vessel.

The bilge keel reduced the roll angles significantly, between 18–40% (model scale comparison). Despite that only one bilge keel was studied and only in model scale, the significant reductions in roll angles show the potential of bilge keels on WTIVs, which justifies further investigations of the concept, i.e., bilge keel sizes and configurations, and the relevance of bilge keels in different operating conditions.

The large deviations between model scale and full scale point out the flaws of experimental tests, namely that it requires large models to reduce scaling effects sufficiently, which makes it expensive to build and conduct. The alternative, the empirical methods, was concluded inappropriate for the considered vessel, which may also apply for other vessels of similar characteristics. Altogether, this emphasizes the strength of using CFD for calculating roll damping and its relevance to optimize the operations of WTIVs to extend their operational weather window, hence pushing the green transition to a faster and safer expansion of renewable energy.

The above conclusions are made based on only one vessel with initial roll angle up to 8°. Future studies should consider other WTIVs and even larger roll angles to represent more severe roll motions.

Abbreviations

The following abbreviations are used in this manuscript:

Base	Base loading condition
BK	Bilge keel
BS	Base size of mesh
CFL	Courant–Friedrichs–Lewy
DOF	Degree of freedom
COG	Center of gravity
HCOG1	Loading condition high center of gravity 1
HCOG2	Loading condition high center of gravity 2
LCOG1	Loading condition low center of gravity 1
LCOG2	Loading condition low center of gravity 2
PS	Prismatic layers
WSPCC	Wide breadth shallow draught pure car carrier
WTIV	Wind turbine installation vessel

CRediT authorship contribution statement

Rasmus Byrdal Kjær: Conceptualization, Methodology, Software, Validation, Formal analysis, Investigation, Writing – original draft, Writing – review & editing, Visualization, Project administration. **Yanlin Shao:** Resources, Writing – review & editing, Supervision. **Jens Honoré Walther:** Resources, Writing – review & editing, Supervision.

Declaration of competing interest

The authors declare that they have no known competing financial interests or personal relationships that could have appeared to influence the work reported in this paper.

Data availability

The data that has been used is confidential.

Acknowledgements

This research has received donations from *OSK Design* and *Cadeler* who have donated materials for building the experimental model. Further, *OSK Design* has donated a substantial part of the required hours for writing this paper. Associate Professor Ulrik Dam Nielsen has supplied motion sensors for the experiments. Lastly, Ph.D. Henrik Mikkelsen has reviewed the manuscript prior to submission.

Funding

This research has received no external funding.

Appendix A. Supplementary data

Supplementary material related to this article can be found online at https://doi.org/10.1016/j.apor.2023.103857.

References

Devolder, B., Stempinski, F., Mol, A., Rauwoens, P., 2020. Roll damping simulations of an offshore heavy lift DP3 installation vessel using the CFD toolbox OpenFOAM. In: Volume 8: CFD and FSI of International Conference on Offshore Mechanics and Arctic Engineering. V008T08A045.

Ding, Y., Walther, J., Shao, Y., 2022. Higher-order gap resonance between two identical fixed barges: a study on the effect of water depth. Phys. Fluids 34, 052113.

Faltinsen, O.M., 1993. Sea Loads on Ships and Offshore Structures. Cambridge University Press.

Gao, J., He, Z., Zang, J., Chen, Q., Ding, H., Wang, G., 2019. Topographic effects on wave resonance in the narrow gap between fixed box and vertical wall. Ocean Eng. 180, 97–107.

Ghamari, I., Mahmoudi, H.R., Hajivand, A., Seif, M.S., 2022. Ship roll analysis using CFD-derived roll damping: Numerical and experimental study. J. Mar. Sci. Appl. 21, 67–79.

Himeno, Y., 1981. Prediction of Ship Roll Damping - State of the Art. University of Michigan, Department of Naval Architecture and Marine Engineering.

Hirt, C., Nichols, B., 1981. Volume of fluid (VOF) method for the dynamics of free boundaries. J. Comput. Phys. 39, 201–225.

Irkal, M.A., Nallayarasu, S., Bhattacharyya, S., 2016. CFD approach to roll damping of ship with bilge keel with experimental validation. Appl. Ocean Res. 55, 1–17.

ITTC Specialist Committee, et al., 2011. Numerical estimation of roll damping, 7.5-02-07-04.5. In: International Towing Tank Conference.

Kawahara, Y., Maekawa, K., Ikeda, Y., 2011. A Simple Prediction Formula of Roll Damping of Conventional Cargo Ships on the Basis of Ikeda's Method and Its Limitation. Springer, Netherlands, Dordrecht, pp. 465–486.

Kianejad, S., Lee, J., Liu, Y., Enshaei, H., 2018. Numerical assessment of roll motion characteristics and damping coefficient of a ship. J. Mar. Sci. Eng. 6, 101.

Lei, W., Chen, J., Shao, Y., Yu, X., 2023. CFD-assisted linearized frequency-domain analysis of motion and structural loads for floating structures with damping plates. Ocean Eng. 281, 114924.

Menter, F.R., 1994. Two-equation eddy-viscosity turbulence models for engineering applications. AIAA J. 32, 1598–1605.

2006. MSC. 1/Circ. In: 1200 Interim Guidelines for Alternative Assessment of the Weather Criterion. International Maritime Organization.

Reichardt, H., 1951. Vollständige darstellung der turbulenten geschwindigkeitsverteilung in glatten leitungen. ZAMM - J. Appl. Math. Mech. / Z. Angew. Math. Mech. 31, 208–219.

Sarpkaya, T., 1986. Force on a circular cylinder in viscous oscillatory flow at low Keulegan-Carpenter numbers. J. Fluid Mech. 165, 61–71.

2021. SESAM, WADAM, Wave Analysis By Diffraction and Morrison Theory, 10.1 ed. DNV, Software user manual.

Shao, Y., Xiang, X., Liu, J., 2019. Numerical investigation of wave-frequency pontoon responses of a floating bridge based on model test results. In: 38th International Conference on Ocean, Offshore & Arctic Engineering, Volume Volume 1: Offshore Technology; Offshore Geotechnics. American Society of Mechanical Engineers, United States.

Siemens, 2022. Simcenter STAR-CCM+ User Guide, 2022.1 ed. Siemens Digital Industries Software, Software user manual.

Standing, R., 1991. Prediction of viscous roll damping and response of transportation barges in waves. In: volume All Days of International Ocean and Polar Engineering Conference. iSOPE-I-91-201.